Received: 15 January 2020 | Revised: 6 April 2020 | Accepted: 7 April 2020
DOI: 10.1002/asl.977

RESEARCH ARTICLE

Atmospheric Science Letters RMetS

A kinetic energy budget on the severe wind production that causes a serious state grid failure in Southern Xinjiang China

Shen-Ming Fu[1] | **Shuang-Long Jin**[2] | **Wei Shen**[3] | **Dan-Yu Li**[4] | **Bin Liu**[4] | **Jian-Hua Sun**[5]

[1]International Center for Climate and Environment Sciences, Institute of Atmospheric Physics, Chinese Academy of Sciences, Beijing, China
[2]State Key Laboratory of Operation and Control of Renewable Energy and Storage Systems, China Electric Power Research Institute, Beijing, China
[3]Power Equipment Status Evaluation Department, Electric Power Research Institute of State Grid Shaanxi Electric Power Company, China
[4]Power Transmission and Transformation Engineering Department, China Electric Power Research Institute, Beijng, China
[5]Laboratory of Cloud–Precipitation Physics and Severe Storms, Institute of Atmospheric Physics, Chinese Academy of Sciences, Beijing, China

Correspondence
Shen-Ming Fu, International Center for Climate and Environment Sciences, Institute of Atmospheric Physics, Chinese Academy of Sciences, Beijing 100029, China.
Email: fusm@mail.iap.ac.cn

Funding information
National Key R&D Program of China, Grant/Award Number: 2018YFC0809400; The National Natural Science Foundation of China, Grant/Award Numbers: 41775046, 41675045; the science and technology foundation of China Electric Power Research Institute, Grant/Award Number: NY83-19-002; The Youth Innovation Promotion Association, Chinese Academy of Sciences

Abstract

Based on the European Centre for Medium-Range Weather Forecasts (ECMWF) ERA5 reanalysis data, in this study, formation mechanisms of a severe windstorm that caused successive trippings of the transmission lines in Southern Xinjiang were investigated. The strong windstorm occurred within a lower-tropospheric warm region due to adiabatic heating of the descending motions ahead of a shortwave trough in the westerly wind (the blocking effects of high mountain was a key reason for the strong descending motions). The kinetic energy (KE) budget indicates two typically different stages appeared in the variation of the windstorm. The former stage showed a rapid wind KE enhancement in the lower troposphere. The KE increase was mainly governed by the downward stretching of high KE (i.e., downward momentum transportation) from the middle troposphere (rather than from the upper-level jet) and the KE production due to the work on rotational wind by the pressure gradient force. The latter stage showed a rapid KE decrease mainly due to the transport of KE by the rotational wind and the pressure gradient force's negative work on the rotational wind. In contrast, the vertical advection of KE still acted as transporting high KE from middle troposphere to lower troposphere, which resisted the KE reduce at the lower levels.

KEYWORDS

Divergent wind, Kinetic energy, Rotational wind, State Grid, Windstorm

1 | INTRODUCTION

In China, the State Grid (SG) has built a large number of transmission lines and power facilities which supply power to more than 1.1 billion population in 26 provinces, autonomous regions, and municipalities, covering 88% of Chinese national territory. Due to its huge coverage, every year, the SG suffers a great loss related to natural disasters. According to Sun *et al.* (2011), over 40% of the total power grid faults are due to natural disasters, with the meteorological disasters occupying the largest proportion. Under the global warming, the meteorological disasters show an obvious increasing trend in causing SG faults (Song *et al.*, 2019). Xie and Li (2006), and Yang *et al.* (2009, 2010) analyzed the natural disasters that cause severe power grid faults in China during recent years, and found that the windstorm was one of the most severe disasters. Similar results are also found in other countries such as Japan and American (Zhang *et al.*, 2015; Cevik *et al.*, 2019; Zhang *et al.*, 2019). In addition to windstorms, lighting, rainstorms, and freezing rain also pose a very big threat to the SG (Xie and Li, 2006; Yang *et al.*, 2010; He *et al.*, 2011; Luo *et al.*, 2016; Song *et al.*, 2019).

Corresponding to the spatial distribution of disaster weathers in China, the SG-related meteorological disasters show significant regional characteristics: lightning activities tend to do more harms to the transmission lines and power facilities in North China and South China (Yang and Sun, 2014; Song *et al.*, 2019); freezing rains tend to cause more damages to the SG in Guizhou and Hunan Provinces (Xie and Li, 2006; Sun and Zhao, 2010), and windstorms tend to induce more SG losses in Southeast China, North China, and Northwest China (Yang *et al.*, 2010; Sun *et al.*, 2011; Zhang *et al.*, 2019). It should be noted that, windstorms in Southeast China, North China and Northwest China are generally associated with different weather systems (Luo *et al.*, 2016; Song *et al.*, 2019). For the former two regions, windstorms mainly appear in the warm season, with the squall lines, multi-cell storms, supercell storms and typhoons being the primary influencing system (Xie and Li, 2006; Markowski and Richardson, 2010; Yang and Sun, 2014; Zhang *et al.*, 2019). In contrast, for Northwest China, windstorms mainly occur in the cold season (Xie and Li, 2006; Sun *et al.*, 2011; Lu *et al.*, 2014). They mainly occur under the influences of extratropical cyclones (Yang and Liu, 2006), middle-level shortwave troughs (Wang *et al.*, 2011; Lu *et al.*, 2014), lower-level highs (Fu *et al.*, 2012), cold fronts (Zhuang *et al.*, 2016), cold waves (Tang *et al.*, 2011), and low-level jets (Li *et al.*, 2012; Zhang *et al.*, 2018). Orographic forcings are confirmed to be a key factor in producing these windstorms by enhancing the low-level pressure gradient (Ding *et al.*, 2019), inducing gravity waves (Lu *et al.*, 2014), causing downslope winds (Zhang *et al.*, 2018) and applying a narrow pipe effect (Wang *et al.*, 2011). Thus far, most previous studies are applied to windstorms in Northern Xinjiang (Tang *et al.*, 2011; Wang *et al.*, 2011; Li *et al.*, 2012; Lu *et al.*, 2014; Zhang *et al.*, 2018; Ding *et al.*, 2019). For Southern Xinjiang, where the geographical features are remarkably different from those of Northern Xinjiang, mechanisms accounting for the development of windstorms still remain vague. Therefore, the primary purpose of this study is to further the understanding of the formation mechanisms of the windstorms in Southern Xinjiang, based on a typical event that caused a serious SG failure around Bachu County (38.7–40.3°N, 77.3–79.9°E). A better understanding of the primary mechanisms underlying the windstorms in Northwest China could provide a better guarantee service for the safe operation of the SG in this region. The remainder of the paper is structured as follows: Section 2 describes the data and analysis methods. Section 3 provides an overview of the event and a corresponding synoptic analysis. Sections 4 show the main results of kinetic energy (KE) budget. Finally, a conclusion and discussion is provided in Section 5.

2 | DATA AND METHOD

In this study, the station observed hourly surface wind was used to analyze the variation of the windstorm. The hourly 0.25° × 0.25° European Centre for Medium-Range Weather Forecasts (ECMWF) ERA5 reanalysis data (Hersbach and Dee, 2016), which has a total of 37 vertical levels, was utilized to conduct a synoptic analysis and a KE budget. The reason why a KE budget was used is that, KE can directly reflect the variation of wind speed, and the KE budget has been proven to be effective in exploring mechanisms underlying wind enhancement (Chen *et al.*, 1978; Fu *et al.*, 2011, 2012). The KE budget equation from Chen *et al.* (1978) was used as following shows:

$$\frac{\partial k}{\partial t} = \underset{\text{TR}}{-\nabla_h \cdot (\mathbf{V}_R k)} \underset{\text{TD}}{-\nabla_h \cdot (\mathbf{V}_D k)} \underset{\text{WR}}{-\mathbf{V}_R \cdot \nabla_h \Phi} \underset{\text{WD}}{-\mathbf{V}_D \cdot \nabla_h \Phi} \underset{\text{TV}}{-\frac{\partial \omega k}{\partial p}} + \text{RES} \tag{1}$$

where $k = \frac{u^2+v^2}{2}$ represents the KE (u and v are zonal and meridional winds, respectively), t is time, ∇_h denotes the horizontal gradient operator, $\mathbf{V}_R$ and $\mathbf{V}_D$ are rotational and divergent wind, respectively, ϕ is the geopotential, p is the pressure, and ω is the vertical speed in *p* coordinate. The rotational and divergent wind are calculated by using the method developed by Xu *et al*. (2011). Terms TR and TD denotes the transport of KE by rotational and divergent wind, respectively; terms WR and WD show the pressure gradient force's work on rotational and divergent wind, respectively; term TV stands for the transport of KE by vertical motion, and term RES means the residual mainly due to friction, subgrid processes and calculation errors. A total (TOT) term is defined as TOT = TR + TD + WR + WD + TV, which represents the overall effects of the right hand side terms except for RES. Sum of TR and TD equals the transport of KE by horizontal wind, and sum of WR and WD equals the pressure gradient force's work on horizontal wind. This means Equation (1) is equivalent to the traditional KE budget method that does not decompose horizontal wind (Markowski and Richardson, 2010). Furthermore, Equation (1) can also show the respective contributions from the vorticity-determined rotational wind and divergence-determined divergent wind (Xu *et al*., 2011). This is useful for a process (such as that in this study) during which divergence and vorticity are notable.

3 | OVERVIEW OF THE EVENT AND SYNOPTIC ANALYSIS

3.1 | Overview of the event

On December 27, 2017, windstorms occurred in Southern Xinjiang (Figure 1a), with the maximum surface wind speed of 9.8 $m \cdot s^{-1}$ observed in the station 51,716 (Figure 1b). In this event, around the Bachu County (the small blue box in Figure 1a), strong wind above 7 $m \cdot s^{-1}$ mainly appeared in the period of 1200 UTC–1400 UTC 27 December (Figure 1b). It is reported that by the SG that, the 750 Kilovolt (KV) transmission line tripped successively from 1100 UTC to 1300 UTC 27 December, within the Bachu County, and the main reason for the line trip was the windstorm. Usually, transmission line trips due to wind deflection are associated with wind speed above 25 $m \cdot s^{-1}$ (Yang and Xu, 2019). What are the formation mechanisms of the windstorm within the Bachu County is the central scientific question for this study. For convenience, a small box which covers the Bachu County (Figure 1a) is determined as the target region for detailed analyses.

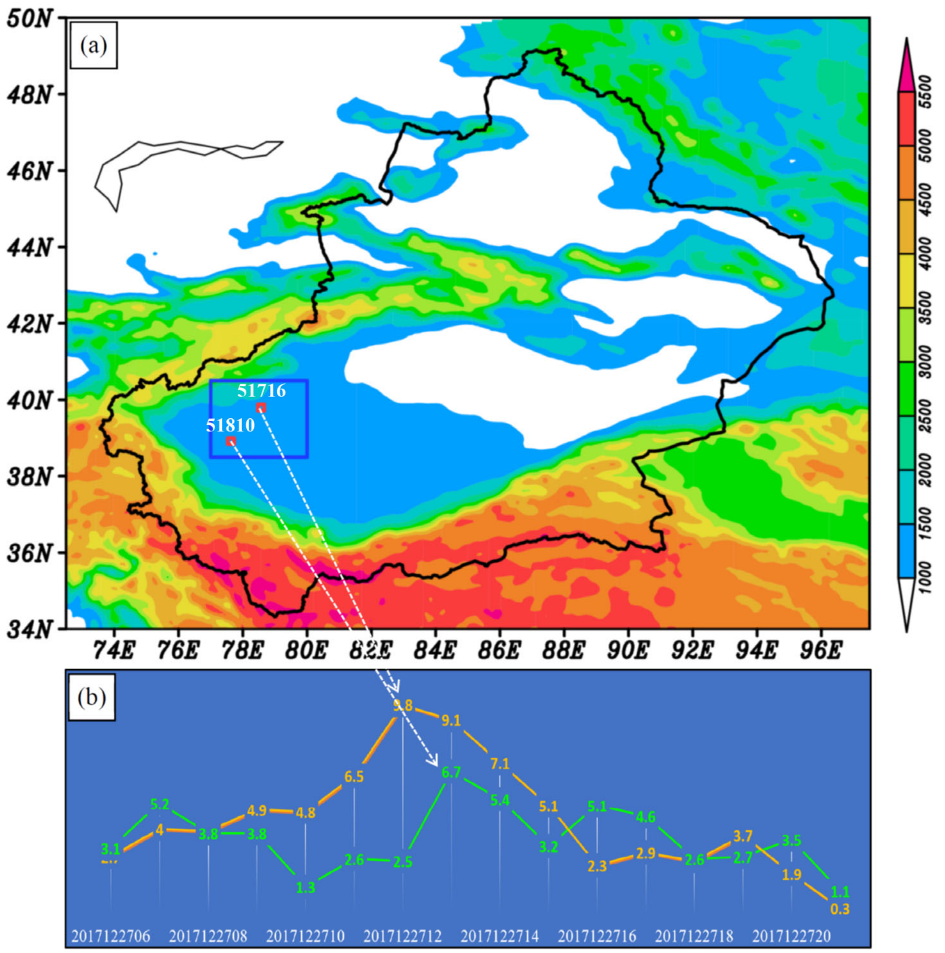

FIGURE 1 Panel (a) shows the terrain features in Xinjiang (shading, units: m), where the big blue box marks the location of the target region, the two small red boxes show the locations of two stations 51,716 and 51,810. Panel (b) shows the observed wind speed (units: $m \cdot s^{-1}$) at the two stations

3.2 | Synoptic analysis

As Figure 2a and b show, in the upper troposphere, the target region was located ahead of a trough. The trough was associated with a warm center of −54°C, with warm temperature advection appeared over the target region (not shown). Ahead of the trough, an upper-level jet appeared and split into two branches, which resulted in

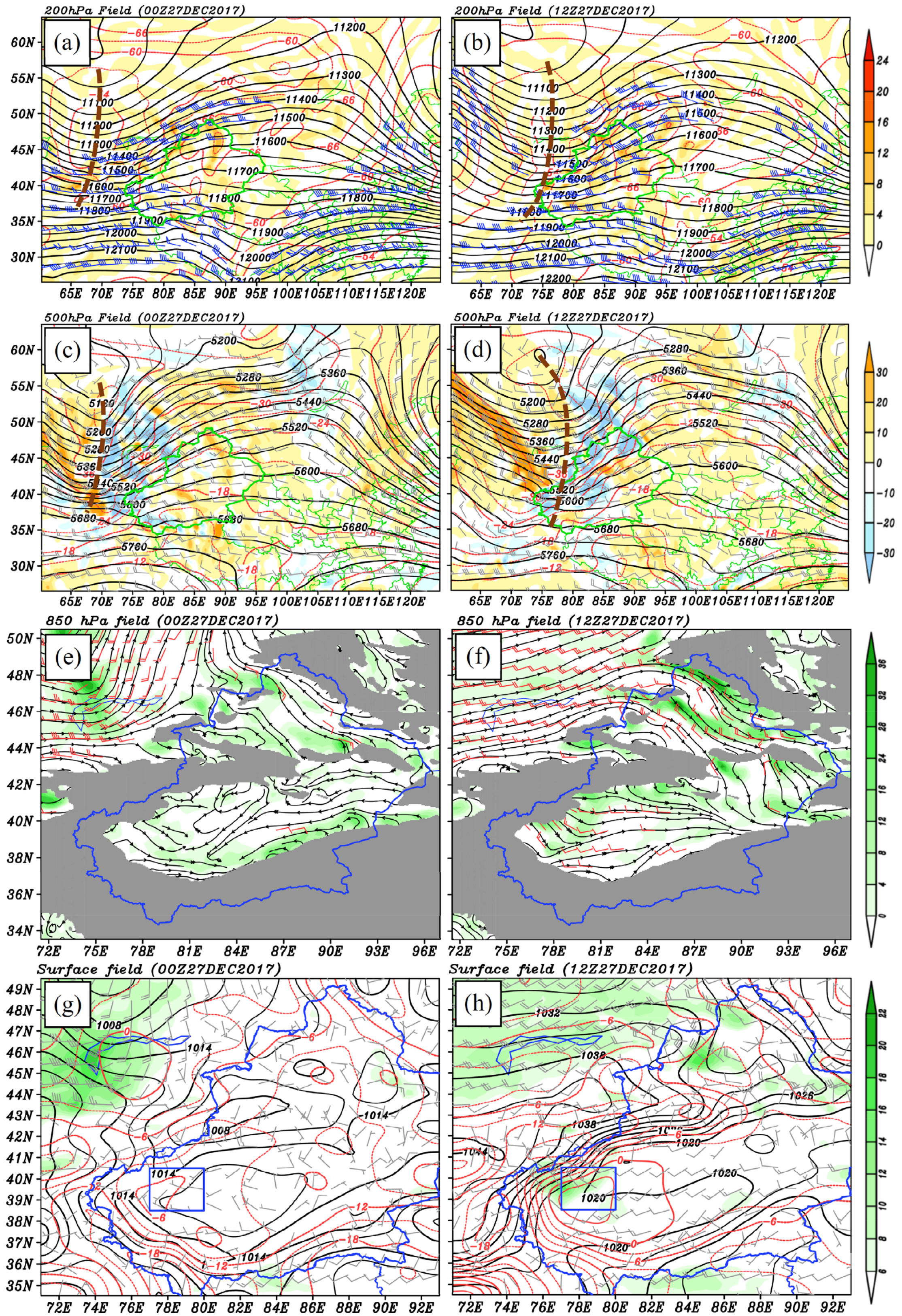

FIGURE 2 Legend on next page.

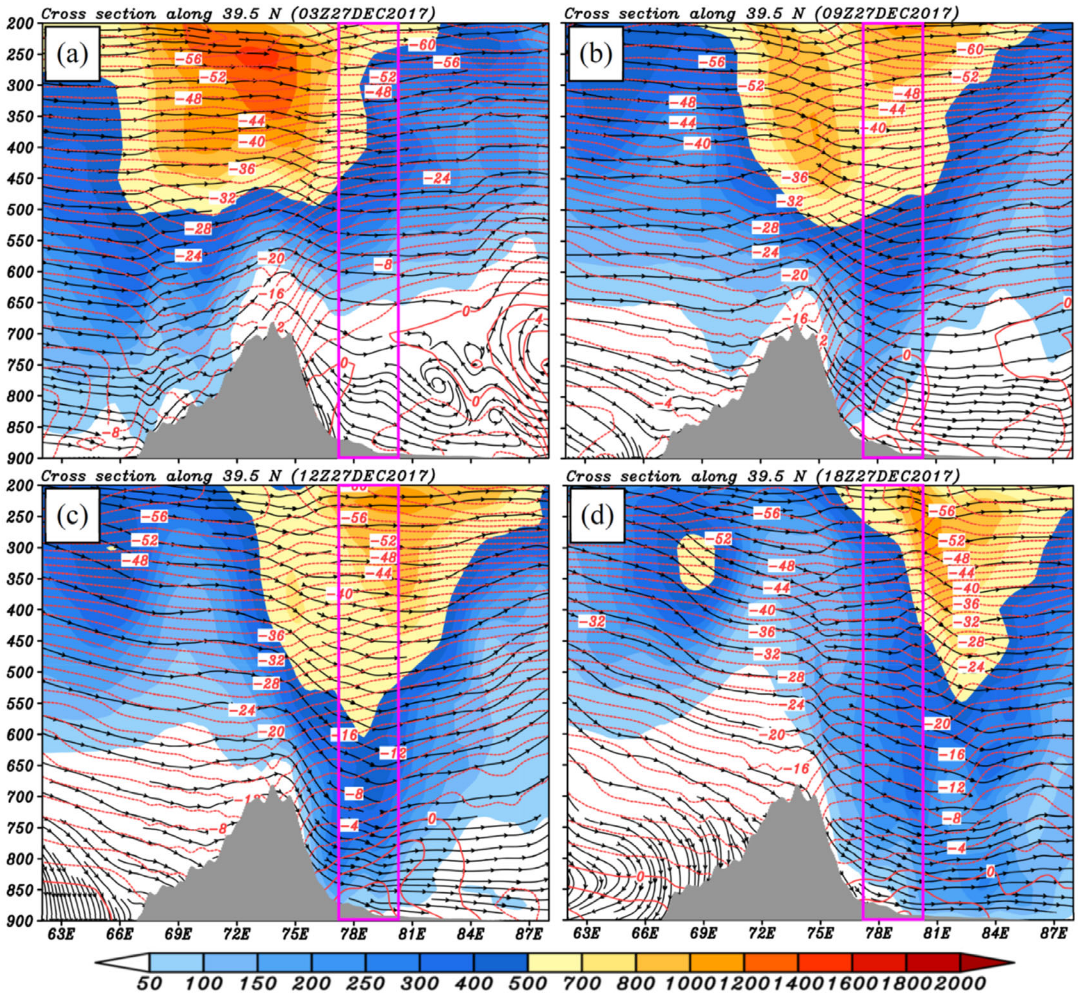

FIGURE 3 Meridional mean (from 38.5°N to 40.5°N) composite of zonal wind and vertical wind (black solid lines with arrows), wind kinetic energy (shading, units: J·kg^{-1}), and temperature (red lines, units: °C), where the gray shading marks the terrain, and the purple boxes mark the target region

strong divergence over the target region (Figure 2b). Overall, warm advection and upper-tropospheric divergence were both favorable for ascending motions. In the middle troposphere, a shortwave trough that was associated with the 200-hPa trough appeared west of Xinjiang (Figure 2c,d). In the central region of the shortwave trough, a cold temperature center appeared, with strong cold temperature advection occurred ahead of the trough line. The target region was located ahead of the shortwave trough, beneath the cold advection (Figure 2d). Generally, cold advection contributed to enhancement of descending motions and lower-level pressure rising (Markowski and Richardson, 2010). Moreover, ahead of the shortwave trough, southwesterly wind was strong, which means the middle-level KE was large (Figure 3). In the lower troposphere, the target region was mainly located in the regions with cyclonic vorticity (Figure 2e,f), with westerly wind enhanced rapidly. In

FIGURE 2 Panels (a and b) show the geopotential height (black solid lines, units: gpm), temperature (red lines, units: °C), wind above 35 m·s^{-1} (a full wind bar represents 10 m·s^{-1}), and divergence (shading, units: 10^{-5}·s^{-1}) at 200 hPa, where the brown dashed lines mark the trough lines. Panels (c and d) show the geopotential height (black solid lines, units: gpm), temperature (red lines, units: °C), wind (a full wind bar represents 10 m·s^{-1}), and temperature advection (shading, units: 10^{-5} K·s^{-1}) at 500 hPa, where the brown dashed lines mark the trough lines. Panels (e and f) show the stream field, wind above 10 m·s^{-1} (a full wind bar represents 10 m·s^{-1}), and vorticity (shading, units: 10^{-5}·s^{-1}) at 850 hPa, where gray shading masks terrain above 1,500 m. panels (g and h) show the wind speed of surface wind (shading, units: m·s^{-1}), mean sea level pressure (black solid lines, units: hPa), surface temperature (red lines, units: °C), and surface wind (a full wind bar represents 4 m·s^{-1}), where the blue boxes mark the target region

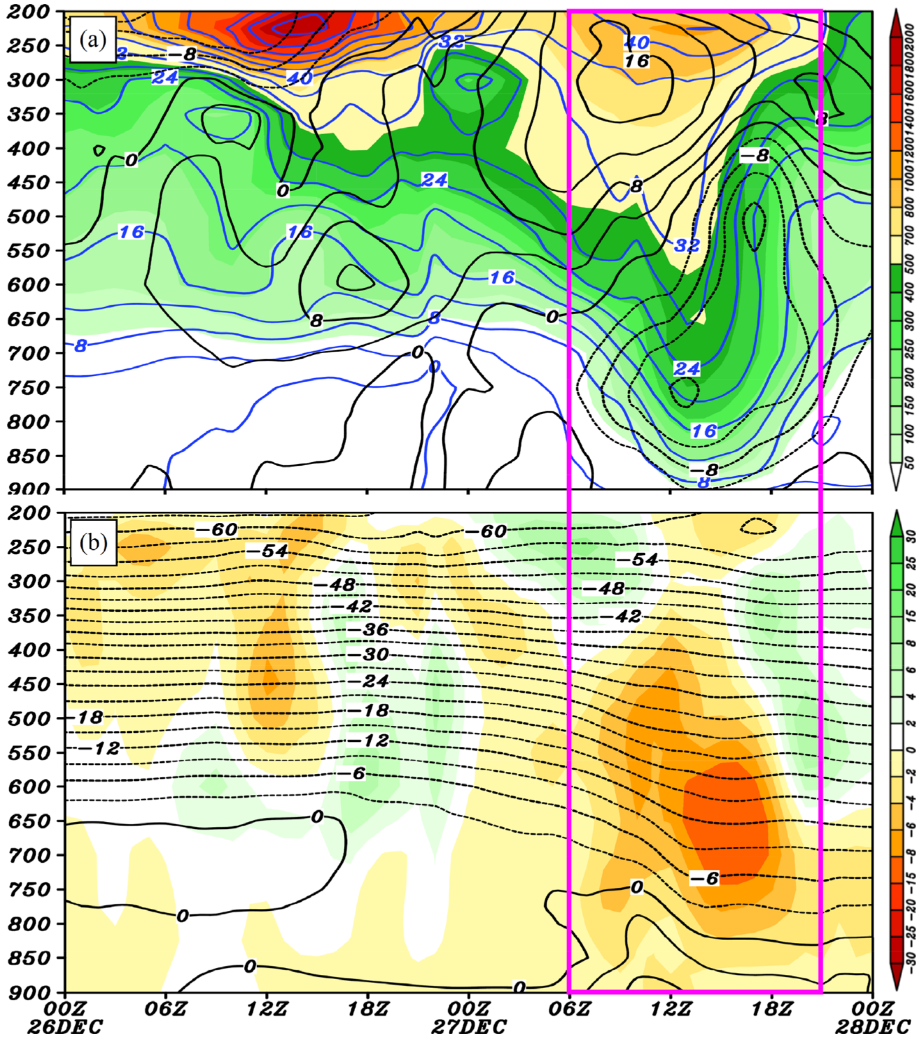

FIGURE 4 Panel (a) shows the target-box averaged wind kinetic energy (shading, units: J·kg^{-1}), zonal wind (blue lines, units: m·s^{-1}) and meridional wind (black lines, units: m·s^{-1}). Panel (b) shows the target-box averaged temperature (black lines, units: °C), and vertical motions (shading, units: cm·s^{-1}). The purple box marks the focused period (from 0600 UTC to 2100 UTC December 2017)

the near surface levels, the target region was located within a warm center northeast of the Pamir Plateau, west of a low-pressure band (Figure 2h), which was governed by a cyclonic circulation. From 0000 UTC to 1200 UTC December 27, 2017, the cyclonic circulation within the target region enhanced with time, as a low-pressure zone developed gradually within the target region (Figure 2g,h). During this process, the southeastward-pointed pressure gradient force within the northern section of the target region increased notably (Figures 2h). It did positive work on the northwesterly wind in this region, which enhanced the wind speed.

From Figures 3a–c, it is obvious that, a lower-tropospheric warm center increased with time (from 0300 UTC to 1,200 UTC 27 December), which accords with the increase of the surface wind during the same period (Figure 1b). The formation of this warm center within the target region was mainly due to the adiabatic descending (according to station observation, no precipitation was observed) after the air flows passed the mountain (Figures 3a–c). The increase of wind speed in the lower troposphere was corresponding to the downward stretching of the large KE region from the middle troposphere. Usually, ahead of a middle-tropospheric shortwave trough, ascending motions are dominant (Markowski and Richardson, 2010; Fu *et al.*, 2012); however, in this event, descending motions were dominant (Figure 3). This is because downslope winds appeared after the lower-level air flow crossed the mountain peak (cf., Figure 3a–c). As documented by Durran (1986), as the air flow ascended along the mountainside, its potential energy was accumulated, and then after the flow passed over the mountain peak and descended along the lee slope, its potential energy was converted into KE, which induced downslope winds.

4 | KINETIC ENERGY BUDGET RESULTS

As the target-region averaged values show, a significant downward stretching of high KE occurred from 0600

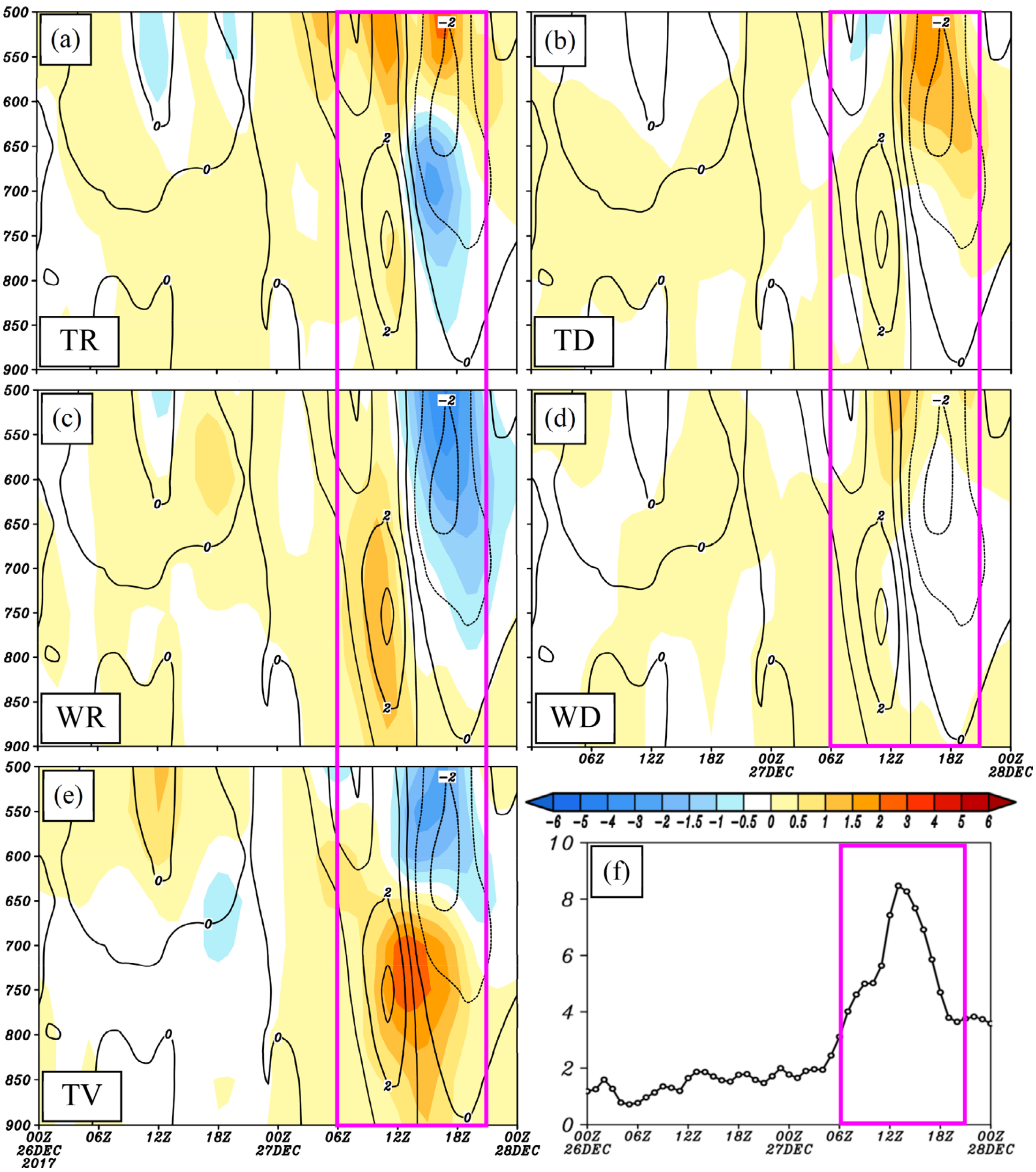

FIGURE 5 Panel (a) shows the target-box averaged TR (shading, units: 10^{-2} W·kg^{-1}), and TOT (black lines, units: 10^{-2} W·kg^{-1}). Panel (b) is the same as (a) but for TD; panel (c) is the same as (a) but for WR; panel (d) is the same as (a) but for WD; and panel (e) is the same as (a) but for TV. Panel (f) is the target-box averaged wind speed (units: m·s^{-1}) at the height of 70 m above the surface. The purple box marks the focused period (from 0600 UTC to 2100 UTC December 2017)

UTC to 2100 UTC 27 December (Figure 4a), which means downward momentum transportation appeared in this region. During the downward stretching process, the westerly wind and northerly wind enhanced rapidly, which was consistent with the observation (not shown). As shown in Figure 4b, strong descending motions were mainly below 450 hPa, while the upper-level jet was mainly located above 400 hPa (Figure 3). Therefore, the downward transfer of momentum of the upper-level jet was not a direct reason for the near-surface wind enhancement in this event, instead, the downward transfer of momentum from the middle troposphere was more important for this event.

Before KE budget analysis, we compared the target-box averaged local time derivative of KE in Equation (1) with the term TOT. It is found that the local time derivative of KE approximately balanced 87% of term TOT (not shown). This means the balance of Equation (1) was good, and thus it could be used for further analysis. From 0600 UTC to 1500 UTC December 2017, a positive TOT appeared within the target region, below 650 hPa (black line in Figure 5a), which was consistent with the rapid KE and wind speed enhancement in the same period (Figures 4a and 5f). The import of KE by the rotational wind (i.e., TR) and divergent wind (i.e., TD) were favorable for the KE increase (Figure 5a,b), with TR having a larger contribution. The work on rotational wind by the pressure gradient force (i.e., WR) (Figure 5c) and the work on divergent wind by the pressure gradient force (i.e., WD) (Figure 5d) both contributed to the KE enhancement, with the former much larger than the latter. The downward transport of KE (i.e., TV) was also conducive to the KE increase below 650 hPa (Figure 5e). Among the five factors mentioned above, terms TV and WR were governing factors for the KE increase. This means that in addition to the downward stretching of high KE from the middle troposphere, the lower-tropospheric KE production due to the work on rotational wind by the pressure gradient force was also very important.

From 1500 UTC to 2100 UTC December 2017, the lower-tropospheric KE (below 650 hPa) within the target region began to reduce in intensity (Figure 4a), as the negative term TOT shows (black lines in Figure 5a). Export of KE from the key region by the rotational wind (Figure 5a) and the work on rotational wind by the pressure gradient force (Figure 5c) dominated this decrease. The transport of KE by the divergent wind (Figure 5b) and the work on divergent wind by the pressure gradient force (Figure 5d) also showed a favorable effect for the KE decrease, but had a much smaller intensity. As the descending motions were notable (Figure 4b), the downward transport of KE from the middle troposphere still remained strong intensity during this stage, which rendered a positive TV (Figure 5e). This effect decelerated the KE decrease in the lower troposphere significantly, which was favorable for the sustainment of strong lower-tropospheric winds.

5 | CONCLUSION AND DISCUSSION

In this study, formation mechanisms of a severe windstorm that caused successive trippings of the transmission lines in Southern Xinjiang were investigated, based on a KE budget analysis using the hourly ECMWF ERA5 reanalysis data. It is found that, the windstorm occurred within the descending motions ahead of a shortwave trough in the westerly wind. This is notably different from the classical ascending motions ahead of a middle-level shortwave trough. In this event, the westerly wind descended after it passed the high terrain west of Xinjiang, which resulted in a lower-level warm center due to adiabatic heating. The warm center modified the pressure field and the associated pressure gradient force within the target region which in turn modified the KE production. The KE budget indicates that two typically different stages appeared in the variation of the windstorm. The first stage showed a rapid wind KE enhancement in the lower troposphere, which was mainly due to the downward stretching of high KE from the middle troposphere and the KE production due to the work on rotational wind by the pressure gradient force. The second stage featured a quick reduce of KE within the key region. Export of KE from the key region by the rotational wind and the work on rotational wind by the pressure gradient force dominated this decrease. The downward transport of KE from the middle troposphere was the only factor that decelerated the KE decrease in the lower troposphere. Compared to previous studies focusing on the windstorms in Northwest China, this event also shows the importance of orographic forcing in modifying the low-level pressure field and enhancing downslope wind (Tang *et al.*, 2011; Wang *et al.*, 2011; Zhang *et al.*, 2018; Ding *et al.*, 2019). However, a downward momentum transportation from the middle troposphere made a notable contribution in this event, whereas it was weak or absent in most previous studies. As a case study, this work has obvious limitations in representing the general mechanisms governing the windstorm formation in Southern Xinjiang. In the future, more cases should be investigated to broaden our understanding of this type of event.

ACKNOWLEDGEMENTS

This research was supported by the National Key R&D Program of China (Grant No. 2018YFC0809400), the National Natural Science Foundation of China (Grant Nos. 41775046; 41675045), the science and technology foundation of China Electric Power Research Institute (Grant No. NY83-19-002), and the Youth Innovation Promotion Association, Chinese Academy of Sciences.

ORCID

Shen-Ming Fu https://orcid.org/0000-0001-9670-0607

REFERENCES

Cevik, H.H., Cunkas, M. and Polat, K. (2019) A new multistage short-term wind power forecast model using decomposition and artificial intelligence methods. *Physica A: Statistical Mechanics and its Applications*, 534, 122177.

Chen, T.-C., Alpert, J.C. and Schlater, T.W. (1978) The effects of divergent and non-divergent winds on the kinetic energy budget of a mid-latitude cyclone: a case study. *Monthly Weather Review*, 108, 458–468.

Ding, J., Chen, Y., Wang, Y. and Xu, X. (2019) The southeasterly gale in Tianshan Grand Canyon in Xinjiang, China: a case study. *Journal of the Meteorological Society of Japan*, 97, 55–67.

Durran, D.R. (1986) Another look at downslope windstorms. Part I: The development of analogs to supercritical flow in an infinitely deep, continuously stratified fluid. *Journal of the Atmospheric Sciences*, 43, 2527–2543.

Fu, S., Sun, J., Zhao, S. and Li, W. (2011) The energy budget of a southwest vortex with heavy rainfall over south China. *Advances in Atmospheric Sciences*, 28, 709–724.

Fu, S.-M., Zhao, S.-X., Sun, J.-H. and Li, W.-L. (2012) Energy budget of a cold surge process during the winter monsoon period of 2004. *Climatic and Environmental Research*, 17, 549–562.

He, Y., Zhu, J., Luo, T. and He, H. (2011) Risk assessment of natural disaster in urban electric power network planning. *Transactions of China Electrotechnical Society*, 26, 205–210.

Hersbach, H. and D. Dee. 2016. *ERA5 reanalysis is in production*. ECMWF Newsletter, No. 147, ECMWF, Reading, 7. Available at: www.ecmwf.int/sites/default/files/elibrary/2016/16299-newsletter-no147-spring-2016.pdf

Li, X., Xia, X.G., Yu, X., Ma, Y.F., Yang, J., Li, J.L. and Yang, X.H. (2012) An examination of boundary layer structure under the influence of the gap winds in Urumqi, China, during air pollution episode in winter. *Journal of the Air & Waste Management Association*, 62, 26–37.

Lu, B., Shi, Y.Q., Wang, G.H. and Yue, B. (2014) Numerical study of severe downslope winds at Kelamayi, XinJiang. *Acta Meteorologica Sinica*, 72, 1218–1230.

Luo, H., Xv, J., Xiao, B., Liu, B., Gong, Z. and Liu, J. (2016) Study on the impact of weather on electricity consumption in Xi-An and its application to mid-long term prediction. *Meteorological Monthly*, 42, 54–60.

Markowski, P. and Richardson, Y. (2010) *Mesoscale Meteorology in Midlatitudes*. Hoboken, NJ: Wiley-Blackwell.

Song, H., Wu, Q., Li, H., Yin, W. and Zhao, W. (2019) Research on the application of meteorological disaster model in power grid transportation inspection business. *Journal of Catastrophology*, 4, 68–72.

Sun, J.-H. and Zhao, S.-X. (2010) The impacts of multi-scale weather systems on freezing rain and snow storms over the southern China. *Weather and Forecasting*, 25, 388–407.

Sun, J., Ge, R., Zheng, L. and Hu, C. (2011) Analysis of state grid security operation in 2010. *Electric Power*, 44, 1–4.

Tang, H.L., Li, R.Q. and Jia, L.H. (2011) Mesoscale numerical simulation of the 28 February 2007 gale in Xinjiang. *Meteorology Monthly*, 37, 1365–1371.

Wang, C.H., Jin, S.L. and Yang, S.L. (2011) Simulation and analysis of the thermal-dynamics characteristics of "2.28" severe wind event in Xinjiang with WRF model. *Journal of Desert Research*, 31, 511–516.

Xie, Q. and Li, J. (2006) Current situation of natural disaster in electric power system and counter measures. *Journal of Natural Disasters*, 15, 126–131.

Xu, Q., Cao, J. and Gao, S. (2011) Computing stream function and velocity potential in a limited domain of arbitrary shape. Part I: Theory and integral formulae. *Advances in Atmospheric Sciences*, 28, 1433–1444.

Yang, X.C. and Liu, X.D. (2006) The relationship between severe dust storms of northern China and the Asian tropospheric wind field. *Climatic and Environmental Research*, 11, 94–100.

Yang, X.-L. and Sun, J.-H. (2014) The characteristics of cloud-to-ground lightning activity with severe thunderstorm wind in south and north China. *Atmospheric and Oceanic Science Letters*, 7, 571–576.

Yang, W.L. and Xu, P.L. (2019) Research on calculation method of windage yaw of large height difference jumper wire under zero-degree wind. *Electric Power Science and Engineering*, 35, 8–13.

Yang, J., Hao, Y., Chen, D. and Jiang, B. (2009) Relationship of power load and weather in agricultural region of Xinjiang. *Meteorological Monthly*, 35, 114–118.

Yang, J., Chen, D., Zhou, Q., Hao, Y. and Jiang, B. (2010) The forecast products of T213 used in power load forecast. *Meteorological Monthly*, 36, 123–127.

Zhang, B., Li, X. and Wang, S. (2015) A novel case adaptation method based on an improved integrated genetic algorithm for power grid wind disaster emergencies. *Expert Systems with Applications*, 42, 7812–7824.

Zhang, G., Zhang, D. and Sun, S. (2018) On the orographically generated low-level easterly jet and severe downslope storms of March 2006 over the Tacheng Basin of Northwest China. *Monthly Weather Review*, 146, 1667–1683.

Zhang, Y., Yang, S., Guo, Z., Guo, Y. and Zhao, J. (2019) Wind speed forecasting based on wavelet decomposition and wavelet neural networks optimized by the Cuckoo search algorithm. *Atmospheric and Oceanic Science Letters*, 12, 107–115.

Zhuang, X., Li, B. and Chen, C. (2016) Analysis of a snowstorm weather process in a coexisting warm area and cold front in northern Xinjiang. *Climatic and Environmental Research*, 21, 17–28.

How to cite this article: Fu S-M, Jin S-L, Shen W, Li D-Y, Liu B, Sun J-H. A kinetic energy budget on the severe wind production that causes a serious state grid failure in Southern Xinjiang China. *Atmos Sci Lett*. 2020;e977. https://doi.org/10.1002/asl.977